Dissociation Dynamics of *n*-Propylbenzene Molecular Ion

Wan Goo Hwang,† Jeong Hee Moon,† Joong Chul Choe,‡ and Myung Soo Kim*,†

National Creative Research Initiative Center for Control of Reaction Dynamics and Department of Chemistry, Seoul National University, Seoul 151-742, Korea, and Department of Chemistry, University of Suwon, Suwon 440-600, Korea

Received: March 2, 1998; In Final Form: June 29, 1998

Production of $C_7H_7^+$ from *n*-propylbenzene molecular ion has been studied using mass-analyzed ion kinetic energy spectrometry. The kinetic energy release distributions in photodissociation and metastable ion decomposition have been determined. The photodissociation rates have been determined also on a nanosecond time scale. All the experimental data could be explained well with the microcanonical transition-state theories when the reaction was assumed to produce only the benzylium ion. Molecular orbital calculations have been carried out to understand the reason for the dominance of the benzylium channel in this system over the tropylium channel, which is important in the dissociation of smaller alkylbenzene ions.

1. Introduction

Production of $C_7H_7^+$ from various molecular ions has been the subject of numerous experimental and theoretical studies in the field of gas-phase ion chemistry.[1−32] This has been investigated using a variety of methods including ordinary mass spectrometry,[1,2] collision-induced dissociation (CID),[3−6] ion cyclotron resonance (ICR),[7−14] photoionization,[15−19] multiphoton ionization,[20] photoelectron−photoion coincidence (PEPICO),[21−24] photodissociation (PD),[25−29] and molecular orbital calculation.[30,31] Recent studies include the determination of the absolute rate constants for the production of $C_7H_7^+$ from various precursor ions such as alkylbenzenes[8,21,27] and halotoluenes[6,9,13,14,25,26] as well as the determination of the isomeric compositions of the reaction products.[4−7,10,13,16,24,26]

Production of $C_7H_7^+$ from alkylbenzene molecular ions displays an interesting trend. Among this series, dissociation of the toluene molecular ion ($C_7H_8^{\bullet+}$), which may be considered as a prototype for the fragmentation chemistry of substituted aromatic ions, has attracted particular attention.[1,5,8,10,17−19,23,24] Investigations over the years have shown that two isomeric ions, namely benzylium (Bz^+) and tropylium (Tr^+), are produced and that the isomerization of the reactant ion between toluene ($TOL^{\bullet+}$) and cycloheptatriene($CHT^{\bullet+}$) structures is rapid at the threshold for the hydrogen atom loss from $C_7H_8^{\bullet+}$.

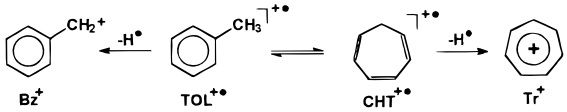

(1)

Even though the above scheme is widely accepted, there have appeared various contradictory claims on the details of the reaction. This is mainly because the physicochemical data obtained with various methods are seemingly contradictory. Recently, Lifshitz and co-workers[17,18] carried out the kinetic analysis of this reaction using the molecular parameters obtained by ab initio calculations. It was shown that most of the physicochemical data could be explained by invoking the case c isomerization/dissociation mechanism of Baer[33] and thermal energy distribution and infrared radiative decay of the reactant. Production of $C_7H_7^+$ from ethylbenzene molecular ion and its derivatives has been investigated also,[2,5,24,28] even though not as extensively as production from $C_7H_8^{\bullet+}$. Isotopic labeling and other studies have shown that the rearrangement of the molecular ions with sufficient internal energy to the cycloheptatriene structure occurs rapidly in this case also.[2,5] Among the higher alkylbenzene ions, dissociation of *n*-butylbenzene molecular ion has been investigated most extensively.[3,11,12,21,27,29] Even though the emphasis of most of the studies was placed on the internal energy dependence of the $[C_7H_7^+]/[C_7H_8^{\bullet+}]$ ratio, it was also found that the loss of $C_3H_7^{\bullet}$ occurred via a simple bond cleavage and only the $C_7H_7^+$ isomer with the benzylium structure was generated.[12,21,27] The fact that the production of the tropylium ion, which may occur via an intermediate with the structure of the cycloheptatriene derivative, is not important in this case is in contrast with the cases of toluene and ethylbenzene molecular ions. Accordingly, it is of interest to study the dissociation dynamics of *n*-propylbenzene molecular ion, which lies between ethylbenzene and *n*-butylbenzene in the alkylbenzene homologue series.

In the present work, $C_2H_5^{\bullet}$ loss of the *n*-propylbenzene ion has been investigated using the nanosecond photodissociation kinetics technique developed in this laboratory.

$$n\text{-}C_6H_5C_3H_7^{\bullet+} \rightarrow C_7H_7^+ + C_2H_5^{\bullet} \qquad (2)$$

As will be shown later, $C_7H_7^+$ generated by reaction 2 has the benzylium structure as for the case of *n*-butylbenzene ion. One advantage in studying the dissociation of *n*-propylbenzene ion over that of *n*-butylbenzene ion is that the rearrangement channel leading to the production of $C_7H_8^{\bullet+}$ is not important. Reduced interference from $C_7H_8^{\bullet+}$ in the experimental data means that the rate constant and the kinetic energy release distribution for the production of $C_7H_7^+$ can be evaluated more reliably. More importantly, the smaller size of *n*-propylbenzene ion compared to *n*-butylbenzene ion allows for the determination of molecular and transition-state structures by quantum chemical calculations, even though at modest levels, which is also included in this work.

* Author to whom correspondence should be addressed.
† Seoul National University.
‡ University of Suwon.

S1089-5639(98)01346-2 CCC: $15.00 © 1998 American Chemical Society
Published on Web 08/28/1998

2. Experimental Section

A double-focusing mass spectrometer with reverse geometry (VG analytical model ZAB-E) modified for photodissociation kinetics study was used in this work. *n*-Propylbenzene was introduced into the ion source via a septum inlet and was ionized by 70 eV electron ionization or by charge exchange using CS_2 as the reagent gas. Ion source temperature was maintained at 180 °C in electron ionization and at 140 °C in charge exchange ionization. Ions generated were accelerated to 8 keV.

Mass-analyzed ion kinetic energy spectrometry (MIKES) was used to observe the dissociation of *n*-propylbenzene molecular ion. Namely, the molecular ion was separated by the magnetic sector, and the translational kinetic energy of a product ion generated in the second field-free region of the instrument was analyzed by the electric sector. Two different modes of dissociation of *n*-propylbenzene ion were investigated. These are the unimolecular or metastable ion decomposition (MID) and the photodissociation (PD). To generate the molecular ions for MID and PD studies, 70 eV electron ionization and charge exchange ionization were used, respectively.

The photodissociation technique developed in this laboratory for the study of ion dissociation dynamics was described in detail previously.[25,34] Briefly, the molecular ion beam was crossed perpendicularly by a laser beam inside an electrode assembly located near the intermediate focal point of the instrument. The 607 nm output of a dye laser (Spectra Physics model 375B), the 514.5 and 488.0 nm lines of an argon ion laser (Spectra Physics model 164-09), and the UV multiple lines (average wavelength of 357 nm) of an argon ion laser (Spectra Physics BeamLok 2065-7s) were used. The laser beam was modulated with a chopper, and phase-sensitive detection was employed. This was to remove the background originating from MID or collision-induced dissociation (CID) by residual gas. The electrode assembly described previously has been slightly modified such that two different modes of operation are possible.[35] In the first mode, high voltage is applied to only one of the electrodes such that the electric field is present in the dissociation region. This enables time-resolved PD study as in the original design. The new design adds the capability to float the dissociation region at high voltage. A PD-MIKE spectrum recorded under this condition, which will be called the voltage-floated PD-MIKE spectrum, allows the determination of the kinetic energy release distribution. With the original design, similar information was obtained by recording a field-off PD-MIKE spectrum. The fact that the interference from the MID and CID backgrounds can be significantly reduced is the advantage of the present design.

To improve the quality of PD- or MID-MIKE spectra, signal averaging was carried out for repetitive scans. Errors quoted in this work were estimated from several duplicate experiments at the 95% confidence limit.

3. Computational Section

The ab initio and semiempirical MO calculations were performed for some important geometries using the Gaussian 94[36] suite of programs on CRAY-T3E LC128/128, and IBM SP2 computers. These include *n*-$C_6H_5C_3H_7^{\bullet+}$, Bz^+, $C_2H_5^\bullet$, ethylcycloheptatriene ion ($ECHT^{\bullet+}$), and intermediates. An attempt was made to find transition states connecting these structures. Special attention was paid to finding the transition state for 1,2 migration. This 1,2 migration transition state corresponds to TS **5**−**11** reported by Lifshitz and co-workers,[17] which was the highest saddle point along the reaction path for $TOL^{\bullet+} \rightleftharpoons CHT^{\bullet+}$ isomerization. Geometries were optimized at the levels of MNDO, HF/3-21G, 6-31G, and 6-31G** with 4.5×10^{-4} hartree/b gradient convergence tolerance. Post-SCF calculation was not attempted because of the excessive computing time required for the transition-state location. TS **5**−**11** for $TOL^{\bullet+} \rightleftharpoons CHT^{\bullet+}$ was also calculated at the same levels. This was to compare the dissociation energetics of *n*-propylbenzene ion with that of toluene ion.

4. Results and Discussion

Investigations on the dissociation of *n*-propylbenzene ion reported so far were made mainly as an attempt to study the structure of the $C_7H_7^+$ product from substituted benzene ions.[4,5,15] No detailed study on its dissociation dynamics has been reported yet. McLoughlin et al.[15] measured the appearance energies for the $C_7H_7^+$ fragment ions from C_1−C_4 monosubstituted alkylbenzenes by photoionization and suggested that the production of $C_7H_7^+$ with the tropylium structure at the threshold is responsible for the low values of the appearance energies measured. In their studies on reaction 1, however, Huang and Dunbar[8] and also Ohmichi and co-workers[19] suggested that the above results are erroneous due to the neglect of the thermal energy of the neutrals. Two CID studies by McLafferty and Winkler[4] and by Buschek et al.[5] suggested that $C_7H_7^+$ formed from *n*-propylbenzene in the ion source is a mixture of benzylium and tropylium. We attempt here to establish that the incipient $C_7H_7^+$ generated from *n*-propylbenzene ion has the benzylium structure based on the rate−energy and kinetic energy release distribution data obtained in this work.

In the MIKE spectrum of the metastable ion decomposition (MID), or MID-MIKE spectrum, of *n*-propylbenzene ion obtained in this work, fragment ions $C_6H_6^{\bullet+}$, $C_7H_7^+$, $C_7H_8^{\bullet+}$, and $C_8H_9^+$ appeared with the relative abundances of 18, 44, 10, and 28%, respectively. In the photodissociation experiments, reaction 2 was found to be the dominant channel. At all the wavelengths used in the present study, the relative abundance of $C_7H_7^+$ in the PD-MIKE spectra was ∼90% of the total fragment ions. The other product ions, $C_6H_6^{\bullet+}$, $C_7H_8^{\bullet+}$, and $C_8H_9^+$, appeared with the relative abundances of 3, 3, and 4%, respectively.

The molecular ion for photodissociation study was generated in the ion source by charge exchange with $CS_2^{\bullet+}$. When the possibility of collisional relaxation in the ion source is ignored, the internal energy of the molecular ion after photoexcitation can be estimated as follows:

$$E = \mathrm{RE} - \mathrm{IE} + E_{\mathrm{th}} + h\nu \qquad (3)$$

Here, RE is the recombination energy of $CS_2^{\bullet+}$ and IE is the ionization energy of *n*-propylbenzene. Their best literature values are 10.07[3] and 8.72[37] eV, respectively. E_{th} is the thermal internal energy at 140 °C. Its distribution was calculated with the molecular parameters in Table 3 according to the well-established method.[25] The most probable internal energies of the *n*-propylbenzene ions thus estimated are 3.63, 4.00, 4.13, and 5.06 eV, respectively, for photodissociation at 607, 514.5, 488.0, and 357 nm. Collisional relaxation in the source was found not to be important for the determination of the kinetic energy release distribution, while a proper correction had to be made for the determination of the rate constant (to be described later). The internal energy of the molecular ion undergoing MID cannot be determined experimentally. Hence, it was estimated from the theoretical rate−energy relation (to be presented later) as follows. The average total rate constant for MID of 3.4×10^4 s^{-1} was estimated from the parent ion transit time ($\tau = 29$

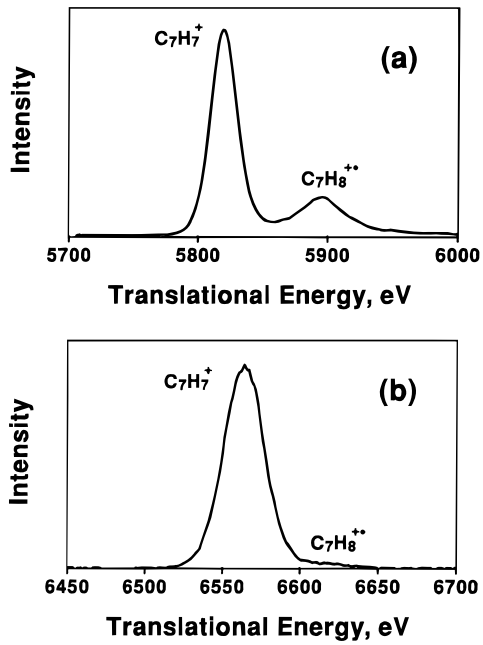

Figure 1. MIKE spectra for $C_2H_5^\bullet$ loss from *n*-propylbenzene ion: (a) MID-MIKE spectrum obtained with the electrode assembly floated at −1.5 kV; (b) PD-MIKE spectrum at 488.0 nm excitation obtained with the electrode assembly floated at 1.5 kV.

± 2 μs). The branching ratio of $C_7H_7^+$ in the MID-MIKE spectrum was multiplied by the above to obtain the average rate constant for the production of $C_7H_7^+$. Then, the internal energy of the parent ion corresponding to the above average rate constant was read from the rate−energy curve. This turned out to be 2.30 eV for MID, occurring near the intermediate focal point of the instrument.

Kinetic Energy Release Distribution (KERD). MIKE profiles of $C_7H_7^+$ generated in MID and PD at 488.0 nm are shown in Figure 1. These profiles were recorded with the dissociation region floated at high voltage as was described in a previous section. The method to evaluate KERD from such MIKE profiles was reported previously.[38] The contamination-free halves of the profiles were used to evaluate KERDs. The results are shown in Figure 2. The average values of the kinetic energy release (KER) were evaluated from the distributions. These were 0.054 and 0.125 eV for MID and PD at 488.0 nm, respectively. The average KERs in PD at other wavelengths were also measured. They are all listed in Table 1.

It is well-known that a large reverse barrier is present in the $CHT^{\bullet+} \rightarrow Tr^+ + H^\bullet$ reaction,[17,18,31] which leads to a large average KER. Our own measurement for MID of $TOL^{\bullet+}$ to $C_7H_7^+$, which is known to generate a large fraction of the tropylium structure, resulted in an average KER of 0.32 eV,[39] which is 6 times larger than the corresponding value for *n*-propylbenzene ion. On the other hand, the production of Bz^+, which would occur by a simple bond cleavage without noticeable reverse barrier, is expected to result in a smaller kinetic energy release than the production of Tr^+. Namely, the small average KERs observed in MID and PD of reaction 2 suggest that the major fraction of $C_7H_7^+$ generated has the benzylium structure. Furthermore, the fact that the KERD curves in Figure 2 display a monotonic pattern, not a bimodal one, indicates that the fraction of Tr^+ is small, if any. In this regard, the KERD in the production of Bz^+ was calculated with a statistical theory and compared with the experimental data.

It is well-known that the phase space theory[40] provides a good description for KERD for dissociation occurring via a loose transition state without a reverse barrier.

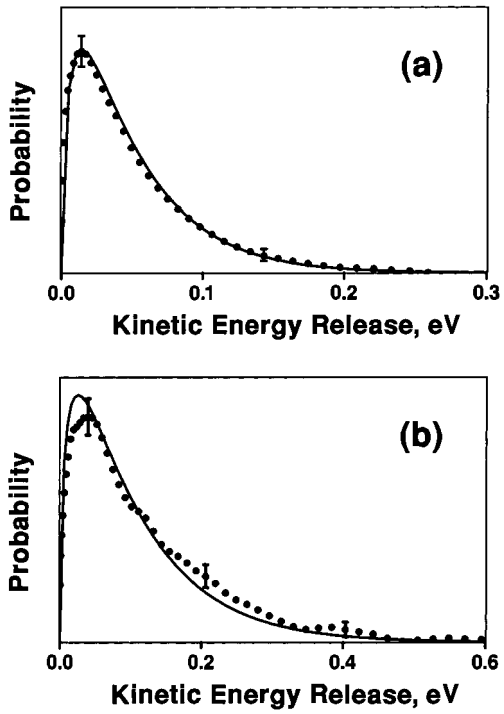

Figure 2. Kinetic energy release distributions for $C_2H_5^\bullet$ loss from *n*-propylbenzene ion: (a) MID and (b) PD at 488.0 nm. Experimental results are shown as filled circles. Theoretical results (phase space theory) are shown as solid curves. Bars represent error limits.

TABLE 1: Kinetic Energy Releases and Rate Constants for Reaction 2

	internal energy (eV)	KER (eV)	rate constant (s^{-1})
	2.28[a]	0.054 ± 0.004	3.4×10^{4} [b]
607 nm	3.63	*c*	$(1.2 \pm 0.9) \times 10^8$
514.5 nm	4.00	0.122 ± 0.012	$(3.6 \pm 0.4) \times 10^8$
488.0 nm	4.13	0.125 ± 0.013	$(4.3 \pm 0.4) \times 10^8$
357 nm	5.06	0.185 ± 0.020	$>8 \times 10^8$

[a] Estimated from the rate−energy curve obtained in the photodissociation study. [b] Estimated from the parent ion transit time. [c] Not determined due to poor signal quality.

$$n(T;J,E) \propto \int_{R_m}^{E-E_0-T} \rho(E-E_0-T-R)P(T,J,R)\,\mathrm{d}R \qquad (4)$$

Here, $n(T; J, E)$ is the KERD at the angular momentum J and the internal energy E. The root-mean-square average J value evaluated at the ion source temperature has been used. ρ and P are the product vibrational and angular momentum state densities, respectively. R is the product rotational energy and R_m is its minimum. E_0 is the reaction critical energy, which may be set equal to the reaction endoergicity at 0 K under the assumption of a completely loose transition state. The value of E_0 evaluated from the best literature thermochemical data,[37,41−43] listed in Table 2, is 1.73 eV. The method to estimate the internal energy E has been presented already. In the case of photodissociation, KERD has been calculated at various internal energies and averaged over the internal energy distribution. Molecular parameters obtained at the HF/6-31G** level (vide infra) were used in the calculation. These are listed in Table 3.

KERDs calculated for MID and PD at 488.0 nm are compared with the experimental data in Figure 2. The agreement between the experimental and theoretical KERDs is excellent, as is seen

TABLE 2: Thermochemical Data

species (structure)	$\Delta H^0_{f,298K}$ (kJ mol^{-1})	$\Delta H^0_{f,0K}$ (kJ mol^{-1})[a]	IE (eV)
n-$C_6H_5C_3H_7$	7.9[b]	44.8	8.72[b]
n-$C_6H_5C_3H_7^{\bullet+}$	849[b]	886	
$C_6H_5CH_2$+(benzylium)	907[c]	926[c]	
$C_2H_5^{\bullet}$	116.3[d]	126.9	

[a] Estimated from 298 K data as described in ref 41. [b] Taken from ref 37. [c] Taken from ref 42. [d] Taken from ref 43.

in the figures. Excellent agreement was also achieved for PD at 357 and 514.5 nm. Upon recollection that the production of Tr^+ would accompany a significant kinetic energy release, it seems safe to conclude that the incipient $C_7H_7^+$ ion generated by reaction 2 has mostly the benzylium structure.

It is to be mentioned that the above conclusion does not mean that $C_7H_7^+$ generated by electron ionization of *n*-propylbenzene in the ion source has the benzylium structure also. This is because the benzylium ion generated with a sufficient internal energy may undergo isomerization to the tropylium structure. The energy barrier for such an isomerization was estimated to be 137 kJ mol^{-1} (1.42 eV) in the MINDO/3 study reported by Cone et al.[31] Then, the $Bz^+ \rightarrow Tr^+$ isomerization may also occur for Bz^+ produced by photodissociation in this study. It is to be noted, however, that such an isomerization does not affect the kinetic energy of $C_7H_7^+$.

Rate−Energy Relation. The PD-MIKE profile for reaction 2 at 514.5 nm obtained with 1.5 kV applied on one of the electrodes in the electrode assembly is shown in Figure 3. The lower energy tail of this profile, which is called the field-on PD-MIKE profile, occurs due to the time delay between photoexcitation and dissociation. The method to obtain the rate constant or its distribution from such a profile was described in detail previously.[44] Briefly, the overall field-on PD-MIKE profile is expressed as a weighted sum of $h(K,t)$, which is the peak shape function for the dissociation occurring at time t.

$$H(K) = \int P(t)h(k,t)\,\mathrm{d}t \tag{5}$$

$h(K,t)$ for each t was derived from the shape of the voltage-floated PD-MIKE profile. Here, K is the translational energy scale in the MIKE spectrum. The probability density for dissociation occurring at time t, $P(t)$, may be expressed as below, assuming the random lifetime distribution and the approximately linear relation between log k and E.

$$P(t) \propto \int P(E)k(E)\mathrm{e}^{-k(E)t}\,\mathrm{d}E \propto \int P(\log k)k\mathrm{e}^{-kt}\,\mathrm{d}\log k \tag{6}$$

$P(E)$ is the internal energy distribution for the photoexcited molecular ion. When a Gaussian-type distribution of the internal energy is assumed, the following analytic expression can be used for $P(\log k)$.

$$P(\log k) \propto \exp[-\alpha(\log k - \log k_c)^2] \tag{7}$$

Here, $\log k_c$ is the most probable value of $\log k$, and α is a constant related to the width of the distribution. k_c corresponds to the rate constant at the most probable internal energy of the photoexcited ion. k_c and α can be determined by a regression analysis of the experimental field-on PD-MIKE profile. In the case of the profile shown in Figure 3, the best k_c and α values were 2.6×10^8 s^{-1} and 6.8, respectively. In our previous photodissociation studies,[26,27,44] the collisional relaxation occurring in the ion source was found to affect the internal energy of the molecular ion and an experimental technique to correct for the relaxation was developed. Following the same procedure, the collisional relaxation-free k_c was estimated by extrapolating the high-pressure data to the zero-pressure limit in this work. The rate constant thus obtained corresponds to the sum of the rate constants for all the competing dissociation channels of the molecular ion. The field-on PD-MIKE profiles of other fragments such as $C_6H_6^{\bullet+}$, and $C_8H_9^+$ were also asymmetrical, even though their quality was not good enough for the determination of the rate constant. Instead of the direct analysis, their field-on PD-MIKE profiles were calculated with the rate constants determined from the $C_7H_7^+$ profiles. A good agreement between the experimental and calculated profiles was achieved, which was taken as the evidence for the competitive production of all the fragment ions. Then, the rate constant for reaction 2 was estimated by multiplying the $C_7H_7^+$ branching ratio by the total rate constant. The photodissociation rate constants for reaction 2 thus obtained are listed in Table 1. For photodissociation at 357 nm the field-on PD-MIKE profile was symmetrical. This means that the dissociation occurs faster than the time resolution of the present technique. The maximum rate constant that can be determined with the present method is estimated to be 8×10^8 s^{-1}.

To interpret the experimental rate−energy data, RRKM-QET[45,46] calculation of the rate constant has been carried out.

$$k(E) = \sigma\frac{W^{\ddagger}(E - E_0)}{h\rho(E)} \tag{8}$$

Here, ρ is the density of states of the reactant, $W^{\ddagger}$ is the state sum at the transition state, and σ is the reaction path degeneracy. Since the difference in the external rotational moments of inertia between the reactant and the transition state is generally ignored, the rotational energy has not been included in the estimation of the reactant internal energy. In a usual RRKM-QET fitting of rate−energy data, the critical energy and the activation entropy at 1000 K ($\Delta S^{\ddagger}$) are treated as two adjustable parameters. In the present case, E_0 was fixed at 1.73 eV, which is the value used in the calculation of KERD and only $\Delta S^{\ddagger}$ was adjusted to fit the experimental data. The best fit was achieved with a $\Delta S^{\ddagger}$ of 35.2 J mol^{-1} K^{-1} as shown in Figure 4. The vibrational frequencies used for the calculation are listed in Table 3. A C−C stretching mode at 1061 cm^{-1} was taken as the reaction coordinate. The calculated rate constant corresponding to photodissociation at 357 nm is 5.0×10^9 s^{-1}, which is larger than the maximum rate constant (8×10^8 s^{-1}) that can be determined with the present method. This agrees with the observation of the symmetrical shape of the field-on PD-MIKE profile at this wavelength.

$\Delta S^{\ddagger}$ of 35.2 J mol^{-1} K^{-1} (=8.42 cal mol^{-1} K^{-1}) indicates that the reaction occurs via a loose transition state. This is in agreement with the simple bond cleavage to the benzylium structure as was concluded in the analysis of KERD. E_0 and $\Delta S^{\ddagger}$ determined here are similar to those (E_0 = 1.61 eV, $\Delta S^{\ddagger}$ = 7.28 cal mol^{-1} K^{-1}) obtained for the production of $C_7H_7^+$ from *n*-butylbenzene ion.[27] It is to be mentioned that the kinetic analysis for the latter reaction led to the conclusion that the $C_7H_7^+$ generated had benzylium structure. The magnitudes of E_0 and $\Delta S^{\ddagger}$ determined in this work may not be so accurate because the experimental rate−energy data are available over a limited time range. Further experimental studies on extended time scales are needed to refine the kinetic parameters.

Molecular Orbital Calculations. Minimum-energy geometries (Figure 5) and energies and vibrational frequencies at these geometries for *n*-propylbenzene ion (NPB$^{\bullet+}$), Bz^+, and $C_2H_5^{\bullet}$

TABLE 3: Molecular Parameters Used in the Calculations of Rate Constants, KERDs, and Internal Energy Distribution

	vibrational frequencies (cm^{-1})[a]
n-$C_6H_5C_3H_7^{\bullet+}$	3059 3055 3047 3042 3039 2954 2951 2942 2915 2899 2880 2876 1601 1491 1476 1463 1461 1457 1419 1400 1362 1337 1324 1290 1280 1257 1201 1173 1164 1117 1061 1046 1005 1002 989 973 959 927 922 856 845 795 778 736 724 623 529 422 418 347 340 290 236 214 82 76 45
TS (NPB$^{\bullet+}$ → $Bz^+ + C_2H_5^{\bullet}$)[b]	3059 3055 3047 3042 3039 2954 2951 2942 2915 2899 2880 2876 1601 1491 1476 1463 1461 1457 1419 1400 1362 1337 1324 1290 1280 1257 1201 1173 1164 1117 1046 1005 1002 989 973 959 927 922 856 845 795 778 736 724 623 529 253 235 217 171 153 132 123 65 52 32
TS **5′**−**11′** [c]	3051 3036 3032 3022 3016 2987 2976 2966 2955 2889 2707 2611 1473 1466 1459 1456 1434 1408 1405 1355 1347 1305 1285 1268 1228 1164 1131 1126 1090 1064 1047 1017 977 950 924 917 911 905 870 829 755 719 670 617 560 544 533 504 428 388 327 272 195 151 109 68
$C_7H_7^+$ (benzylium)	3091 3063 3060 3041 3039 3034 2998 1595 1559 1552 1463 1431 1336 1321 1318 1166 1143 1120 1097 1054 1020 1008 983 971 953 849 788 784 633 616 587 514 410 345 340 164
$C_2H_5^{\bullet}$	3064 2970 2925 2876 2839 1459 1448 1437 1383 1166 997 963 784 316 155

	rotational constants (cm^{-1})[d]			polarizability (10^{-24} cm^3) [d]
n-$C_6H_5C_3H_7^{\bullet+}$	0.139	0.0292	0.0259	
$C_7H_7^+$	0.179	0.0945	0.0620	
$C_2H_5^{\bullet}$	3.51	0.753	0.699	6.22

[a] The HF/6-31G** results multiplied by 0.90. [b] Estimated value. [c] See text for the definition. The HF/6-31G** results for the MNDO geometry multiplied by 0.90. [d] The HF/6-31G** results.

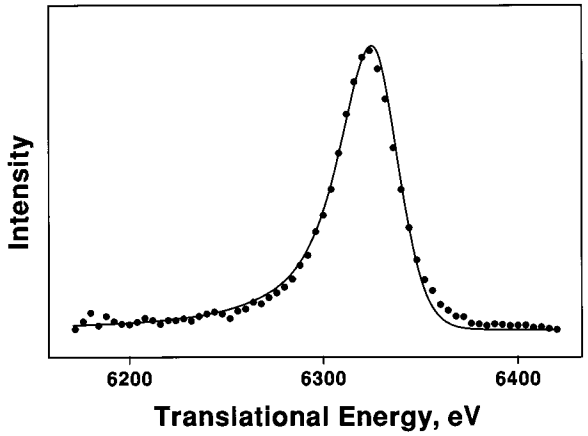

Figure 3. PD-MIKE spectrum at 514.5 nm for $C_2H_5^{\bullet}$ loss from *n*-propylbenzene ion obtained with 1.5 kV applied on one of the electrodes in the electrode assembly. Experimental and calculated results are shown as filled circles and a solid curve, respectively. A slight discrepancy between the two results at the high translational energy side is due to the production of $C_7H_8^{\bullet+}$.

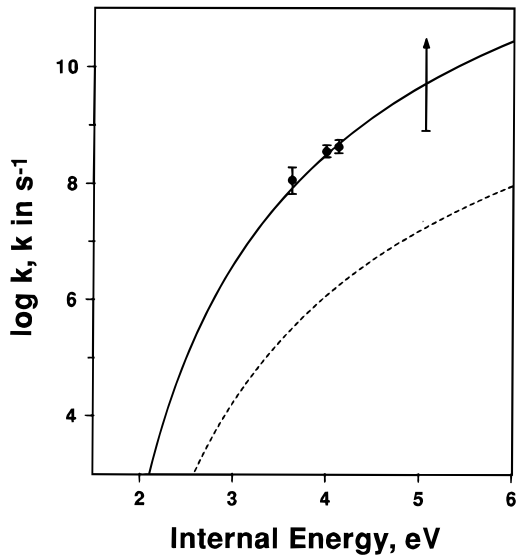

Figure 4. Rate−energy dependence for $C_2H_5^{\bullet}$ loss from *n*-propylbenzene ion. Experimental results are shown as filled circles. The result for the photodissociation at 357 nm is shown as an arrow. The theoretical result (RRKM-QET) is shown as the solid curve. Rate parameters used in the calculation are $E_0 = 1.73$ eV and $\Delta S^{\ddagger} = 35.2$ J mol^{-1} K^{-1} (8.42 cal mol^{-1} K^{-1}). Bars represent error limits. The dashed curve is a rough RRKM-QET estimate of the rate−energy dependence for the isomerization to ECHT$^{\bullet+}$ calculated with $E_0 = 1.72$ eV and the vibrational frequencies for NPB$^{\bullet+}$ and TS **5′**−**11′** in Table 3.

were calculated. Attempts were made at various calculation levels to obtain the potential energy curve between NPB$^{\bullet+}$ and the ethylcycloheptatriene (ECHT$^{\bullet+}$) structure and between ECHT$^{\bullet+}$ and $Tr^+ + C_2H_5^{\bullet}$. Saddle points were located, and the intrinsic reaction coordinates (IRCs) were calculated to confirm that a particular saddle point found was connected to the reactant, product, or intermediates. Such an effort was partially successful at the MNDO level, and the reaction to Tr^+ and Bz^+ is presumed to occur via the following mechanism.

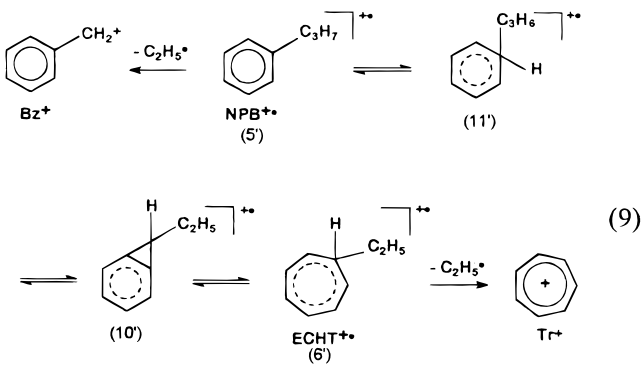

(9)

Structures of the intermediate **11′** and the saddle point TS **10′**−**6′** could not be determined due to the computational difficulty. Notations for the stable structures and the transition states have been taken from Dewar and Landman.[47] The saddle point **5′**−**11′** is equivalent to TS **5**−**11** in the TOL$^{\bullet+}$ ⇌ CHT$^{\bullet+}$ isomerization reported by Lifshitz and co-workers.[17] Similar saddle points, namely TS **5′**−**11′**, could be found at Hartree−Fock levels (Figure 6). To confirm that these are the transition-state structures for the NPB$^{\bullet+}$ → ECHT$^{\bullet+}$ isomerization, the intrinsic reaction coordinates (IRCs) were calculated also. It was found that these structures led to the NPB$^{\bullet+}$ structure via the backward reaction. The forward IRC calculations in the Hartree−Fock levels were not successful, however, due to the presence of tiny local minima near the saddle points. Namely, these saddle points may not be the true transition states even though their structures look similar to the one found at the MNDO level. Then, the energies at the true transition state

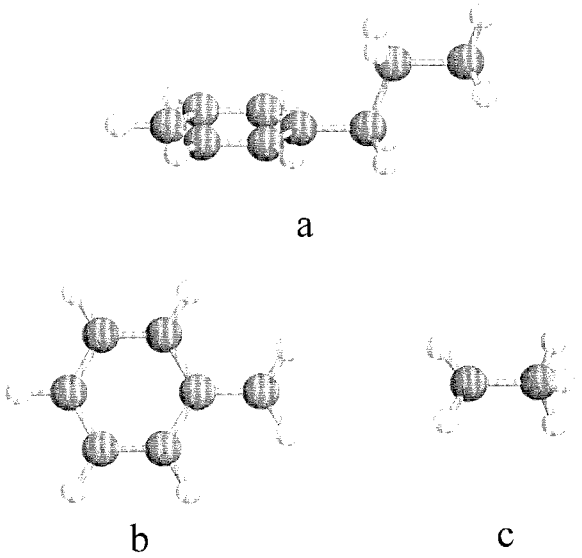

Figure 5. Minimum-energy geometries for *n*-propylbenzene ion ($NPB^{\bullet+}$), Bz^+, and $C_2H_5^\bullet$ calculated at the HF/6-31G** level.

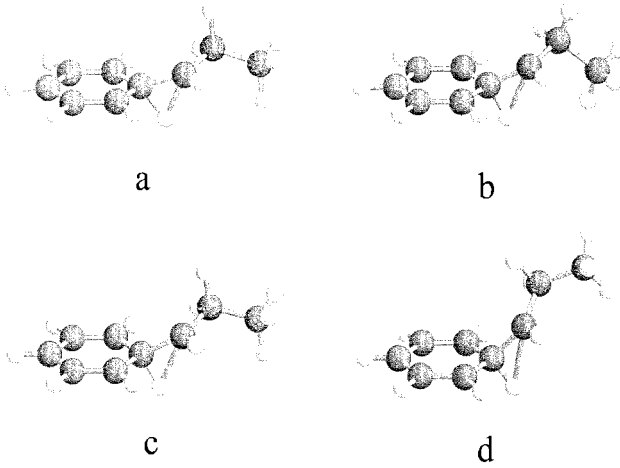

Figure 6. Structures at the saddle point located between $NPB^{\bullet+}$ and the ethylcycloheptatriene ($ECHT^{\bullet+}$) found at various levels (a) MNDO, (b) HF/3-21G, (c) 6-31G, and (d) 6-31G**, respectively.

may be higher than those of the above saddle points. The Hartree−Fock calculations were also done for the MNDO transition-state geometry. At a given HF level, the energy difference between the saddle point found at this level and the MNDO transition-state structure was around 0.1 eV. The zero-point energy correction was made for the minimum-energy and saddle-point geometries. The usual 10% correction for the vibrational frequencies was made for the HF level calculations, while the correction factors reported by Dewar and co-workers[48] were utilized for the MNDO results. Then, the critical energy for the production of Bz^+ ($E_0(NPB^{\bullet+} \rightarrow Bz^+)$) was evaluated as the difference between the energies of $Bz^+ + C_2H_5^\bullet$ and $NPB^{\bullet+}$. The critical energy for the isomerization to $ECHT^{\bullet+}$, $E_0(NPB^{\bullet+} \rightarrow ECHT^{\bullet+})$, was evaluated using two different estimates of the transition-state energy, the one obtained at the saddle point found at that ab initio level and the other obtained by the ab initio calculation for the MNDO transition-state geometry. Similar calculations were performed for the corresponding reactions of $TOL^{\bullet+}$ for comparison. In the case of $TOL^{\bullet+}$, there was no ambiguity in the determination of the transition state for the isomerization. The four critical energies, $E_0(NPB^{\bullet+} \rightarrow Bz^+)$, $E_0(NPB^{\bullet+} \rightarrow ECHT^{\bullet+})$, $E_0(TOL^{\bullet+} \rightarrow Bz^+)$, and $E_0(TOL^{\bullet+} \rightarrow CHT^{\bullet+})$, thus obtained are listed in Table 4.

TABLE 4: Critical Energies (in eV) for the Production of Bz^+ and the Isomerization to the Cycloheptatriene Structure from Toluene and *n*-Propylbenzene Ions Calculated at Various Levels

	$E_0(TOL^{\bullet+} \rightarrow Bz^+)$	$E_0(TOL^{\bullet+} \rightarrow CHT^{\bullet+})$	$E_0(NPB^{\bullet+} \rightarrow Bz^+)$	$E_0(NPB^{\bullet+} \rightarrow ECHT^{\bullet+})$
MNDO	2.30	1.82	0.94	1.45
HF/3-21G	2.12	1.91	1.49	1.55[a]/1.64[b]
HF/6-31G	2.10	1.92	1.30	1.55[a]/1.60[b]
HF/6-31G**	2.23	1.93	1.48	1.57[a]/1.47[b]
exptl	2.26[c]		1.73[c]	

[a] Calculated using the energy of the saddle point obtained at this level. [b] Calculated using the energy of the MNDO transition-state structure obtained at this level. [c] Estimated with the thermochemical data for reactants and products in Table 2 and ref 37.

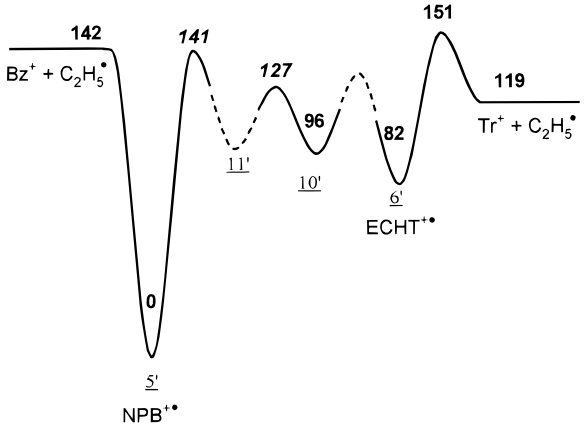

Figure 7. Schematic potential-energy diagram for $C_2H_5^\bullet$ loss from *n*-propylbenzene ion. Notations for the structures follow those by Dewar and Landman.[47] The boldface numbers denote the energy in kJ mol^{-1} referred to the energy minimum of $NPB^{\bullet+}$. All energies were calculated at the HF/6-31G** level. The italic boldface numbers denote the energies calculated at the HF/6-31G** level for the MNDO geometries.

It is seen that the critical energy for the production of Bz^+ from $TOL^{\bullet+}$ is consistently higher than the isomerization barrier to $CHT^{\bullet+}$. This is in qualitative agreement with the results of Lifshitz and co-workers.[17] Even though there is some uncertainty in the evaluation of the isomerization barrier in the case of $NPB^{\bullet+}$, it is higher than the critical energy for the production of Bz^+ at most of the levels of calculation with the exception of the HF/6-31G** calculation at the MNDO transition-state geometry. Namely, the simple bond cleavage to Bz^+ seems to be energetically more favorable than or comparable to the rearrangement to $ECHT^{\bullet+}$ in the case of *n*-propylbenzene ion.

A schematic potential-energy diagram for the production of Bz^+ and Tr^+ from $NPB^{\bullet+}$ is shown in Figure 7. Energies of $NPB^{\bullet+}$, Bz^+, $ECHT^{\bullet+}$, Tr^+, $C_2H_5^\bullet$, the intermediate **10′**, and the transition state between $ECHT^{\bullet+}$ and $Tr^+ + C_2H_5^\bullet$ are those calculated at the HF/6-31G** level. Energies of TS **5′**−**11′** and TS **11′**−**10′** are those calculated at the HF/6-31G** level for the transition-state geometries found at the MNDO level. It is to be noted that the energy of TS **5′**−**11′** in this diagram is slightly lower than that of $Bz^+ + C_2H_5^\bullet$, while the opposite is the case at other calculation levels.

It is well-known that in the competition between a simple bond cleavage and a rearrangement, the former becomes more favorable as the reactant internal energy increases. Then, the formation of Bz^+ can be preferred to that of isomerization to $ECHT^{\bullet+}$ in the present case, in agreement with the experimental results. To confirm this, a simple RRKM-QET calculation of the rate−energy relation for the isomerization to $ECHT^{\bullet+}$ has been carried out. Calculation has been done utilizing the

transition-state property evaluated at the HF/6-31G** level for the MNDO structure. The calculated critical energy for the isomerization is smaller by 1 kJ mol^{-1} than the corresponding value for the benzyl channel. Since the critical energy of 1.73 eV was adopted for the RRKM calculation of the latter channel, 1.72 eV has been taken as the critical energy for the isomerization channel. Vibrational frequencies of the transition state calculated at the HF/6-31G** level for the MNDO structure have been used after 10% correction. These are listed in Table 3. The rate−energy relation for the isomerization thus calculated is compared with that for the production of Bz^+ in Figure 4. It is seen that the rate constant for the production of Bz^+ is larger than that for the isomerization by more than 2 orders of magnitude over the reactant internal energy range of 2.3−5.1 eV covered in the present work.

5. Conclusion

Dissociation dynamics of *n*-propylbenzene ion to $C_7H_7^+$ has been investigated by the metastable ion decomposition and photodissociation methods. Comparison of the experimental KERDs with those calculated with the statistical phase space theory has shown that the incipient $C_7H_7^+$ ion has the benzylium structure over the reactant internal energy range of 2.3−5.1 eV investigated in this work. The fact that KERD in the production of benzylium ion can be predicted accurately by the phase space theory suggests that KERD can play an important role in the structural determination of $C_7H_7^+$ ions generated from benzene derivative ions. The rate−energy relation on the nanosecond time scale determined by the photodissociation kinetics technique also supported the production of the benzylium ion. This does not mean, however, that the benzylium structure will be retained after a prolonged time. This is because the benzylium-to-tropylium isomerization may occur for the benzylium ion generated with a sufficient internal energy.

The result from the present investigation establishes an interesting trend in the production of $C_7H_7^+$ from *n*-alkylbenzene ions. Namely, the simple bond cleavage to Bz^+ is the dominant channel in the dissociation of *n*-propylbenzene and *n*-butylbenzene ions. On the other hand, the isomerization to the cycloheptatriene structure and subsequent dissociation to the tropylium ion are important for toluene and ethylbenzene ions. Molecular orbital calculations carried out at the limited level of accuracy suggest that the relative heights of the barriers to the simple bond cleavage and isomerization are responsible for the above experimental trend. Quantum chemical study of the toluene and ethylbenzene ion systems at high ab initio levels will be useful for a better understanding of the $C_7H_7^+$ production mechanism. Also useful will be the measurement and/or prediction of KERD in the production of Tr^+ from $CHT^{\bullet+}$. These are being attempted as a continuation of the present study.

Acknowledgment. This work was supported financially by CRI, the Ministry of Science and Engineering, Republic of Korea.

References and Notes

(1) Cooks, R. G.; Beynon, J. H.; Bertrand, M.; Hoffman, M. K. *Org. Mass Spectrom.* **1973**, *7*, 1303.

(2) Grotemeyer, J.; Grützmacher, H.-F. *Org. Mass Spectrom.* **1982**, *17*, 353.

(3) Nacson, S.; Harrison, A. G. *Int. J. Mass Spectrom. Ion Processes* **1985**, *63* 325.

(4) McLafferty, F. W.; Winkler, J. *J. Am. Chem. Soc.* **1974**, *96*, 5182.

(5) Buschek, J. M.; Ridal, J. J.; Holmes, J. L. *Org. Mass Spectrom.* **1988**, *23*, 543.

(6) Olesik, S.; Baer, T.; Morrow, J. C.; Ridal, J. J.; Buschek, J.; Holmes, J. L. *Org. Mass Spectrom.* **1989**, *24*, 1008.

(7) Jackson, J.-A. A.; Lias, S. G.; Ausloos, P. *J. Am. Chem. Soc.* **1977**, *99*, 7515.

(8) Huang, F.-S.; Dunbar, R. C. *Int. J. Mass Spectrom. Ion Processes* **1991**, *109*, 151.

(9) Lin, C. Y.; Dunbar, R. C. *J. Phys. Chem.* **1994**, *98*, 1369.

(10) Dunbar, R. C. *J. Am. Chem. Soc.* **1975**, *97*, 1382.

(11) Uechi, G. T.; Dunbar, R. C. *J. Chem. Phys.* **1992**, *96*, 8897.

(12) Chen, J. H.; Hays, J. D.; Dunbar, R. C. *J. Phys. Chem.* **1984**, *88*, 4759.

(13) Shin, S. K.; Han, S.-J.; Kim, B. *Int. J. Mass Spectrom. Ion Processes* **1996**, *157/158*, 345.

(14) Kim, B.; Shin, S. K. *J. Chem. Phys.* **1997**, *106*, 1411.

(15) McLoughlin, R. G.; Morrison, J. D.; Traeger, J. C. *Org. Mass Spectrom.* **1979**, *14*, 104.

(16) Lifshitz, C.; Levin, I.; Kababia, S.; Dunbar, R. C. *J. Phys. Chem.* **1991**, *95*, 1667.

(17) Lifshitz, C.; Gotkis, Y.; Ioffe, A.; Laskin, J.; Shaik, S. *Int. J. Mass Spectrom. Ion Processes* **1993**, *125*, R7.

(18) Lifshitz, C. *Acc. Chem. Res.* **1994**, *27*, 138.

(19) Ohmichi, N.; Gotkis, I.; Steens, L.; Lifshitz, C. *Org. Mass Spectrom.* **1992**, *27*, 383.

(20) Lablanquie, P.; Ohashi, K.; Nishi, N. *J. Chem. Phys.* **1993**, *98*, 399.

(21) Baer, T.; Dutuit, O.; Mestdagh, H.; Rolando, C. *J. Phys. Chem.* **1988**, *92*, 5674.

(22) Baer, T.; Morrow, J. C.; Shao, J. D.; Olesik, S. *J. Am. Chem. Soc.* **1988**, *110*, 5633.

(23) Bombach, R.; Dannacher, J.; Stadelmann, J.-P. *J. Am. Chem. Soc.* **1983**, *105*, 4205.

(24) Ausloos, P. *J. Am. Chem. Soc.* **1982**, *104*, 3259.

(25) Choe, J. C.; Kim, M. S. *J. Phys. Chem.* **1991**, *95*, 50.

(26) Cho, Y. S.; Kim, M. S.; Choe, J. C. *Int. J. Mass Spectrom. Ion Processes* **1995**, *145*, 187.

(27) Oh, S. T.; Choe, J. C.; Kim, M. S. *J. Phys. Chem.* **1996**, *100*, 13367.

(28) Mukhtar, E. S.; Griffiths, I. W.; March, R. E.; Harris, R. M.; Beynon, J. H. *Int. J. Mass Spectrom. Ion Phys.* **1981**, *41*, 61.

(29) Welch, M. J.; Pereles, D. J.; White, V. E. *Org. Mass Spectrom.* **1985**, *20*, 425.

(30) Abboud, J.-L. M.; Hehre, W. J.; Taft, R. W. *J. Am. Chem. Soc.* **1976**, *98*, 6072.

(31) Cone, C.; Dewar, M. J. S.; Landman, D. *J. Am. Chem. Soc.* **1977**, *99*, 372.

(32) Kuck, D. *Mass Spectrom. Rev.* **1990**, *9*, 187.

(33) Baer, T.; Brand, W. A.; Bunn, T. L.; Butler, J. J. *Faraday Discuss. Chem. Soc.* **1983**, *75*, 45.

(34) Choe, J. C.; Kim, M. S. *Int. J. Mass Spectrom. Ion Processes* **1991**, *107*, 103; *J. Phys. Chem.* **1992**, *96*, 726.

(35) Lim, S. H.; Choe, J. C.; Kim, M. S. Submitted for publication.

(36) Frisch, M. J.; Trucks, G. W.; Schlegel, H. B.; Gill, P. M. W.; Johnson, B. G.; Robb, M. A.; Cheeseman, J. R.; Keith, T.; Petersson, G. A.; Montgomery, J. A.; Raghavachari, K.; Cioslowski, J.; Stefanov, B. B.; Nanayakkara, A.; Challacombe, M.; Peng, C. Y.; Ayala, P. Y.; Chen, W.; Wong, M. W.; Andres, J. L.; Replogle, E. S.; Gomperts, R.; Martin, R. L.; Fox, D. J.; Binkley, J. S.; Defrees, D. J.; Baker, J.; Stewart, J. P.; Head-Gordon, M.; Gonzalez, C.; Pople, J. A. *Gaussian 94*, revision E.2; Gaussian, Inc.: Pittsburgh, PA, 1995.

(37) Lias, S. G.; Bartmess, J. E.; Liebman, J. F.; Holmes, J. L.; Levine, R. D.; Mallard, W. G. *J. Phys. Chem. Ref. Data* **1988**, *17* (Suppl. 1).

(38) Yeh, I. C.; Kim, M. S. *Rapid Commun. Mass Spectrom.* **1992**, *6*, 115, 293.

(39) Hwang, W. G.; Choe, J. C.; Kim, M. S. Unpublished result.

(40) Chesnavich, W. J.; Bowers, M. T. *J. Am. Chem. Soc.* **1976**, *98*, 8301; *J. Chem. Phys.* **1977**, *66*, 2306; *Prog. React. Kinet.* **1982**, *11*, 137.

(41) Traeger, J. C.; McLoughlin, R. G. *J. Am. Chem. Soc.* **1981**, *103*, 3647.

(42) Ellison, G. B.; Davico, G. E.; Bierbaum, V. M.; Depuy, C. H. *Int. J. Mass Spectrom. Ion Processes* **1996**, *156*, 109.

(43) Holmes, J. L.; Lossing, F. P.; Maccoll, A. *J. Am. Chem. Soc.* **1988**, *110*, 7339.

(44) Yim, Y. H.; Kim, M. S. *J. Phys. Chem.* **1993**, *97*, 12122.

(45) Rosenstock, H. M.; Wallenstein, M. B.; Wahrafitig, A. L.; Eyring, H. *Proc. Natl. Acad. Sci. U.S.A.* **1952**, *38*, 667.

(46) Robinson, P. J.; Holbrook, K. A. *Unimolecular Reactions*; Wiley-Interscience: London, 1972.

(47) Dewar, M. J. S.; Landman, D. *J. Am. Chem. Soc.* **1977**, *99*, 2446.

(48) Dewar, M. J. S.; Ford, G. P.; McKee, M. L.; Rzepa, H. S.; Thiel, W.; Yamaguchi, Y. *J. Mol. Struct.* **1978**, *43*, 135.